IEEE Robotics and Automation Letters (RAL) paper presented at the
2020 IEEE International Conference on Robotics and Automation (ICRA)
31 May - 31 August, 2020. Paris, France

Nonholonomic Virtual Constraint Design for Variable-Incline Bipedal Robotic Walking

Jonathan C. Horn, Alireza Mohammadi, Kaveh Akbari Hamed, and Robert D. Gregg

***Abstract*— This paper presents a method of designing relative-degree-two nonholonomic virtual constraints (NHVCs) that allow for stable bipedal robotic walking across variable terrain slopes. Relative-degree-two NHVCs are virtual constraints that encode velocity-dependent walking gaits via momenta conjugate to the unactuated degrees of freedom for the robot. We recently introduced a systematic method of designing NHVCs, based on the hybrid zero dynamics (HZD) control framework, to achieve hybrid invariant flat ground walking without the use of dynamic reset variables. This work addresses the problem of walking over variable-inclined terrain disturbances. We propose a methodology for designing NHVCs, via an optimization problem, in order to achieve stable walking across variable terrain slopes. The end result is a single controller capable of walking over variable-inclined surfaces, that is also robust to inclines not considered in the optimization design problem, and uncertainties in the inertial parameters of the model.**

I. Introduction

Despite the recent breakthroughs in bipedal robotic locomotion, biological biped walking still outperforms its robotic counterpart in terms of agility, robustness to rough terrain, and achieving task diversity. Indeed, walking across various terrains and a wide variety of irregular surfaces is a trivial task for most humans. On the other hand, overcoming the challenge of moving in unknown or varying terrain environments is still an open problem in the field of autonomous bipedal robots [1]–[5] as well as powered prostheses/orthoses [6]–[8], where the aim is to restore healthy human walking across various terrain profiles.

To address the issue of biped walking over uneven ground, several modelling and control frameworks have been proposed thus far [9]–[17]. The first group of these control schemes relies on a finite collection of gaits designed by optimization or human data collection, where each gait corresponds to a particular task. The goal is then to drive the robot to a predefined periodic gait by using non-periodic transitional gaits [9], or to interpolate in between the pre-defined gaits using techniques such as supervised machine learning [10], [11], low-rank kinematic models [14], or control barrier functions [13]. The second group of control schemes for realizing walking across various terrain profiles relies on online optimization of walking gaits. To accommodate velocity disturbances, hybrid zero dynamics (HZD)-based stable walking gaits are optimized online using Legendre pseudo-spectral methods in [18]. Online gait generation has also been leveraged through adaptive foot positioning to generate stable walking gaits in the presence of perturbations in [19], [20]. However, these two groups of solutions share a common limitation of requiring estimates of the terrain or some *a priori* knowledge of the environment.

The final family of control schemes, which are known as nonholonomic virtual constraints (NHVCs), encode velocity-dependent stable walking gaits via momenta conjugate to the unactuated degrees-of-freedom of the bipedal robot [16], [17], [21], [22]. NHVCs have been shown to be statistically more robust than virtual holonomic constraints (VHCs) [21], and have been shown to be robust to a wide variety of external perturbations [16], [17]. In other words, NHVCs do not require explicit knowledge of the terrain to update the controller at each step. Therefore, this work will seek to leverage NHVCs in order to design a single controller that is capable of stable walking over sloped terrain disturbances.

Contributions of the paper: Using the notion of relative degree-two NHVCs, which were first introduced in [16], [17] and later formalized in [21], we extend the class of NHVCs in [21] to account for multiple terrain slopes during walking. The extended NHVCs are designed to remain stable for a finite collection of terrain disturbances and slopes without employing a dynamic variable as in [16], where a discrete variable gets updated after each impact with the ground in order to guarantee stable walking under NHVCs. Furthermore, we cast the variable-incline NHVC design problem as an optimization, where the energy expenditure over one step is minimized while stable walking for finitely many distinct terrain slopes is guaranteed simultaneously. The obtained *single* NHVC walking gait, in turn, results in a *single* controller capable of ensuring stable walking over a finite set of slopes without the need for real-time slope detection or computationally expensive schemes of changing control structure, machine learning, online optimization, or dynamic reset variables.

The rest of the paper is organized as follows. Sec. II reviews the preliminaries from the HZD framework and the notion of NHVCs. Sec. III presents an optimization-based methodology for designing a single NHVC for multiple

This work was supported by NSF Award 1652514/1949869 and 1637704/1854898. R. D. Gregg IV, Ph.D., holds a Career Award at the Scientific Interface from the Burroughs Wellcome Fund.

J. C. Horn is with the Department of Mechanical Engineering and Department of Bioengineering, University of Texas at Dallas, Richardson, TX 75080, USA. jch160630@utdallas.edu

A. Mohammadi is with the Department of Electrical & Computer Engineering, University of Michigan, Dearborn, MI 48128, USA. amohmmad@umich.edu

K. Akbari Hamed is with the Department of Mechanical Engineering, Virginia Tech, Blacksburg, VA 24061, USA. kavehakbarihamed@vt.edu

R. D. Gregg is with the Department of Electrical Engineering and Computer Science and the Robotics Institute, University of Michigan, Ann Arbor, MI 48109 USA. rdgregg@umich.edu

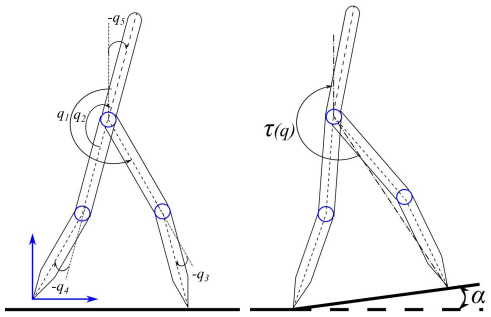

Fig. 1: Diagram of the 5-link planar biped robot RABBIT on flat and sloped ground [24].

possible Poincaré sections, each corresponding to a different ground inclination. Sec. IV presents a simulation study of an underactuated 5-link planar biped with an example NHVC design for a level, downhill, and uphill incline. This study verifies the ability of the biped to seamlessly transition between these designed inclines, compares the controllers ability to navigate continuously varying terrain surfaces with other traditional approaches, and examines the sensitivity of the proposed control scheme in the presence of model uncertainties. Finally, Sec. V provides concluding remarks and future research directions stemming from this work.

II. Preliminaries

In this section we briefly review the dynamics of planar bipedal robots with one degree of underactuation. Also, we briefly review the class of NHVCs that are used in this work [16], [21]. The presented material on planar bipedal dynamics and HZD framework in this section is standard, and the reader is referred to [23] for further details.

Notation. Given two vectors (matrices) a, b, we denote by $[a;b]$ the vector (matrix) $[a^T, b^T]^T$ where $(\cdot)^T$ is the transpose operator. Given a function $h : \mathcal{X} \to \mathcal{Y}$, we define its zero levelset via $h^{-1}(0) := \{x \in \mathcal{X} : h(x) = 0\}$.

A. Hybrid Dynamics Underactuated Bipedal Robots

Continuous Dynamics. We consider an inertial world frame rigidly attached to level ground. During the swing phase, the biped robot dynamics in this frame are given by (see [25]),

$$M(q)\ddot{q} + C(q,\dot{q})\dot{q} + G(q) = Bu, \tag{1}$$

the Lagrangian, $\mathcal{L}$: $TQ \to \mathbb{R}$, is $\mathcal{L}(q,\dot{q}) = K(q,\dot{q})$-$V(q)$, with K and V representing the biped kinetic and potential energy functions, respectively. In (1), $q := [q_1; ...; q_N] \in Q$ is the vector of generalized coordinates, the configuration space Q is an open and connected subset of $\mathbb{R}^N$, and TQ denotes the tangent bundle of the mechanical system. Therefore, the state $x := [q;\dot{q}]$ of the biped belongs to the state space $\mathcal{X} = TQ := Q \times \mathbb{R}^N$. The matrix, $B \in \mathbb{R}^{N\times(N-1)}$, is assumed to be constant and of full rank and the vector of torque inputs, u, belongs to an open and connected subset of $\mathbb{R}^{N-1}$. This assumption implies that there exists a row vector $B^\perp \in \mathbb{R}^{1\times N}$ such that $B^\perp B = 0$. The unactuated coordinate is then defined by

$$q_u := B^\perp q. \tag{2}$$

Finally, $M(q), C(q,\dot{q})$, and $G(q)$, denote the inertia and Coriolis/centripetal matrices, and the vector of gravitational forces, respectively. We also assume that the inertia matrix is not a function of the unactuated DOF, which is known as a *cyclic variable*. That is, $(\partial M/\partial q_u)(q) = 0$ for all $q \in \mathcal{Q}$. Essentially, if a given variable q_N is cyclic for a pinned open kinematic chain, the kinetic energy remains invariant under rotation of the inertial frame [23].

Impact Dynamics. We let $p_2^v(q)$ and $p_2^h(q)$ denote the vertical height from the ground and the horizontal position of the swing leg end, with respect to the inertial coordinate frame, respectively. An autonomous system with impulsive effects will consist of three things: 1) An autonomous ordinary differential equation that is defined for some state space, $\mathcal{X}$, 2) A hyper surface, $\mathcal{S}$, where solutions of the differential equation are subject to a discrete transition, and 3) A rule, $\Delta : \mathcal{S} \to \mathcal{X}$ that specifies the new initial conditions with respect to the point at which the solution impacts $\mathcal{S}$. Note that Δ resets (re-labels) the configuration and the joint velocities through an instantaneous change. However, since we are considering multiple ground slopes, the hypersurface will be parameterized by the angle of the ground slope (α) such that

$$\mathcal{S}_\alpha := \{(q,\dot{q}) \in \mathcal{X} : p_2^v(q) - \tan(\alpha)p_2^h(q) = 0, p_2^h(q) > 0\}. \tag{3}$$

Therefore, $\mathcal{S}_\alpha$ is denoted as the switching surface corresponding to the Poincaré section of a particular ground slope (see Fig. 2). In this work, we assume that the leg impacts with the ground are perfectly inelastic [26]. Under this assumption, the impact is modeled by

$$[q^+;\dot{q}^+] = [\Delta_q(q^-); \Delta_{\dot{q}}(q^-)\dot{q}^-], (q^-,\dot{q}^-) \in \mathcal{S}_\alpha, \tag{4}$$

that is invariant under the slope α. Also, it is important to note that $\Delta_q(q^-)$ is a vector and $\Delta_{\dot{q}}(q^-)$ is a matrix. Here, $[q^-;\dot{q}^-]$ and $[q^+;\dot{q}^+]$ are the states of the robot just before and after impact, respectively. The overall biped hybrid dynamics (1) – (4) can be described by

$$\Sigma_\alpha : \begin{cases} \dot{x} = f(x) + g(x)u, & x^- \notin \mathcal{S}_\alpha \\ x^+ = \Delta(x^-), & x^- \in \mathcal{S}_\alpha \end{cases} \tag{5}$$

where $\Delta(x) := [\Delta_q(q); \Delta_{\dot{q}}(q)\dot{q}]$, $g(x) := [0; M^{-1}(q)B]$, and $f(x) := [\dot{q};\ M^{-1}(q)(-C(q,\dot{q})\dot{q} - G(q))]$.

B. Nonholonomic Virtual Constraints

We utilize the momenta conjugate to the unactuated DOF to construct nonholonomic constraints as in [16], [17], [21]. It is the momentum that is only affected by the conservative forces acting on the biped robot mechanism (due to its potential energy) and not the control inputs. The momentum conjugate to the unactuated DOF, q_u, is defined as

$$\sigma_u(q,\dot{q}) := \frac{\partial \mathcal{L}}{\partial \dot{q}_u}(q,\dot{q}) = B^\perp M(q)\dot{q}, \tag{6}$$

and, from the Euler-Lagrange equations, satisfies

$$\frac{d}{dt}\sigma_u(q,\dot{q}) = \frac{\partial \mathcal{L}}{\partial q_u}(q). \tag{7}$$

It can be seen that $\partial\mathcal{L}/\partial q_u$=$(1/2)\dot{q}^T(\partial M/\partial q_u)\dot{q} - \partial V/\partial q_u$ depends only on the configuration variables. Indeed,

$$\frac{\partial \mathcal{L}}{\partial q_u}(q) = -\frac{\partial V}{\partial q_u}(q). \tag{8}$$

A **nonholonomic virtual constraint (NHVC)** for the biped robot dynamics in (1)–(4) is expressed as an output function of the form

$$y = h(q, \sigma_u(q, \dot{q})) \in \mathbb{R}^{N-1}. \tag{9}$$

By construction, taking one time derivative of (9) and using (7), it can be seen that,

$$\dot{y} = \frac{\partial h}{\partial q}(q, \sigma_u(\cdot))\dot{q} + \frac{\partial h}{\partial \sigma_u}(q, \sigma_u(\cdot))\frac{\partial \mathcal{L}}{\partial q_u}(q). \tag{10}$$

Therefore, this choice of output results in the input u only appearing after taking two time derivatives of the output. That is, we have constructed the NHVCs such that the outputs will have relative-degree-two. This in turn allows for influence over both the joint positions and velocities.

C. Feedback Control Design

Since we are interested in making the NHVCs invariant with respect to the biped robot dynamics, we define

$$\begin{aligned}\mathcal{Z} :=& \{(q, \dot{q}) \in T\tilde{Q} : h(q, \sigma_u(\cdot)) = 0, \\ & \frac{\partial h}{\partial q}(q, \sigma_u(\cdot))\dot{q} + \frac{\partial h}{\partial \sigma}(q, \sigma_u(\cdot))\frac{\partial \mathcal{L}}{\partial q_u}(q) = 0\},\end{aligned} \tag{11}$$

where $(\cdot)$ denotes $(q, \dot{q})$. $\mathcal{Z}$ is denoted as the zero dynamics manifold, and will be used in the problem formulation for the optimization.

The feedback controller presented in this work is designed in the same way as [21], and follows the method of [27]. For the biped RABBIT [24], we define four virtual constraints for each actuator of the system. Therefore, the output vector $y : Q \times I \to \mathbb{R}^{N-1}$ is a function of the momenta conjugate to the unactuated coordinate, σ_u, and the configuration variables, q. Here $I \subset \mathbb{R}$ is an open and connected set. In order to find the control torque, u^*, that makes the manifold $\mathcal{Z}$ invariant, we start by taking the time derivative of (10) along the system trajectories. We obtain

$$\ddot{y} = \frac{\partial h}{\partial q}\ddot{q} + \frac{d}{dt}(\frac{\partial h}{\partial q})\dot{q} + \frac{d}{dt}(\frac{\partial h}{\partial \sigma})\frac{\partial \mathcal{L}}{\partial q_u} + \frac{\partial h}{\partial \sigma}\frac{d}{dt}(\frac{\partial \mathcal{L}}{\partial q_u}). \tag{12}$$

Hence, we can obtain the u^* that will yield $\ddot{y} = -k_d\dot{y} - k_p y$ by substituting (1) into (12) and solving for u^*. After a lengthy calculation, we arrive at

$$\begin{aligned}u^*(q, \dot{q}) = A^{-1}(q, \sigma_u(\cdot))\{&\frac{\partial h}{\partial q}M^{-1}(q)(C\dot{q} + G(q)) \\ -\frac{d}{dt}(\frac{\partial h}{\partial q})\dot{q} - \frac{d}{dt}(\frac{\partial h}{\partial \sigma})\frac{\partial \mathcal{L}}{\partial q_u} &- \frac{\partial h}{\partial \sigma}\frac{d}{dt}(\frac{\partial \mathcal{L}}{\partial q_u}) - k_d\dot{y} - k_p y\},\end{aligned} \tag{13}$$

where $A(q, \sigma_u(\cdot)) = (dh/dq)M^{-1}(q)B$ is the decoupling matrix. In (13), we introduce the terms $k_d\dot{y}$ and $k_p y$ to stabilize the output, where the positive definite matrices k_p, k_d contain the proportional and derivative gains.

III. Nonholonomic Virtual Constraint Design

This section presents the methodology for the design and control NHVCs that will enable hybrid invariance for multiple Poincaré sections. In this section, we will formulate an optimization problem that systematically designs a unified nonholonomic virtual constraint controller to address walking on different slopes.

To formalize the notion of hybrid invariance across multiple Poincaré sections, let us consider a finite set of possible slope angles for the terrain as $\mathcal{A} := \{\alpha_i\}_{i=1}^m$ that includes level ground, i.e., $0 \in \mathcal{A}$. Suppose further that we have designed a family of holonomic outputs, using the same method as presented in [23], each corresponding to one particular slope angle. We consider the holonomic output $h_{\text{h},\alpha_i}(q)$ for the slope α_i, where the subscript "h" stands for holonomic. The I-O linearizing controller for the holonomic output is denoted by $u_{\text{h},i}(x)$ that renders the corresponding zero dynamics manifold $\mathcal{Z}_{\text{h},\alpha_i}$ attractive and invariant under the flow of the closed-loop system. We further assume that manifold $\mathcal{Z}_{\text{h},\alpha_i}$ is hybrid-invariant on slope α_i, i.e., each output $h_{\text{h},\alpha_i}(q)$ is designed such that $\mathcal{S}_{\alpha_i} \cap \mathcal{Z}_{\text{h},\alpha_i} \neq \emptyset$ and $\Delta(\mathcal{S}_{\alpha_i} \cap \mathcal{Z}_{\text{h},\alpha_i}) \subset \mathcal{Z}_{\text{h},\alpha_i}$. Furthermore, we assume that there is an exponentially stable periodic solution (i.e., orbit) for the closed-loop system that represents steady-state walking on the slope α_i (we denote it by $\mathcal{O}_{\text{h},\alpha_i}$). Due to this specific construction, $\mathcal{O}_{\text{h},\alpha_i} \subset \mathcal{Z}_{\text{h},\alpha_i}$. In addition, we assume that the holonomic fixed point

$$\{x^\star_{\text{h},\alpha_i}\} := \bar{\mathcal{O}}_{\text{h},\alpha_i} \cap \mathcal{S}_{\alpha_i}, \quad \forall \alpha_i \in \mathcal{A}, \tag{14}$$

is a singleton, where $\bar{\mathcal{O}}_{\text{h},\alpha_i}$ represents the set closure of $\mathcal{O}_{\text{h},\alpha_i}$.

Using the family of holonomic outputs h_{α_i}, our objective is to design a unified nonholonomic output that addresses walking for all angles $\alpha_i \in \mathcal{A}$. For this purpose, let us consider the following parameterized form of (9)

$$y(q, \sigma_u, b, \kappa) := \sum_{i=1}^{m} b_i\, h_{\text{h},\alpha_i}(q) - h_{\text{nh}}(\sigma_u, \kappa), \tag{15}$$

where $b := \text{col}\{b_1, \cdots, b_m\}$ represents a set of coefficients for the linear combination of $h_{\text{h},\alpha_i}(q)$. Additionally, $h_{\text{nh}}(\sigma_u, \kappa)$ is an $\mathcal{M}$-th order Bézier polynomial given by

$$h_{\text{nh}}(\sigma_u, \kappa) := \sum_{n=0}^{\mathcal{P}} \kappa_n \frac{\mathcal{P}!}{n!(\mathcal{P}-n)!}\sigma_u^n(1-\sigma_u)^{\mathcal{P}-n}. \tag{16}$$

Here $\kappa := [\kappa_0\, \kappa_1\, \cdots\, \kappa_M]$ represents the coefficient matrix of the Bézier polynomial. It is important to note that Bézier polynomials possess special properties (e.g., they are contained in the convex hull of their defined control points), however Bézier polynomials are not strictly necessary for this algorithmic construction. In addition, we assume that $u_{\text{nh}}(x, b, \kappa)$ denotes the I-O linearizing controller for the parameterized output $y(q, \sigma_u, b, \kappa)$. The corresponding zero dynamics manifold, which can be computed using (11), is represented by $\mathcal{Z}_{\text{nh},\beta,\kappa}$. In what follows, we first compute the Poincaré map associated with the NHVC in (15), and then

use it for setting up the design procedure of the parameters κ and b via an optimization problem.

The solution of the smooth closed-loop ODE $\dot{x} = f^{\text{cl}}(x, b, \kappa) := f(x) + g(x)\, u_{\text{nh}}(x, b, \kappa)$ with the initial condition x_0 is denoted by $\varphi(t, x_0, b, \kappa)$ for all $t \geq 0$ in the maximal interval of existence. For every α, the time-to-impact function is defined as the first time at which the state solution $\varphi(t, x_0, \beta, \kappa)$ meets the guard $\mathcal{S}_\alpha$, that is,

$$T(x_0, b, \kappa, \alpha) := \inf\{t > 0 \,|\, \varphi(t, x_0, b, \kappa) \in \mathcal{S}_\alpha\}. \tag{17}$$

For every two angles $\alpha, \beta \in \mathcal{A}$ with the property $\alpha > \beta$, the flow extension map is defined as $\mathcal{F}(., b, \kappa, \beta) : \mathcal{S}_\alpha \to \mathcal{S}_\beta$ by

$$\mathcal{F}(x, b, \kappa, \beta) := \varphi\left(T(x, \kappa, \beta), x, b, \kappa\right) \tag{18}$$

that represents the state solution evaluated on $\mathcal{S}_\beta$ while starting from $x \in \mathcal{S}_\alpha$. The Poincaré return map is also defined as $P(., b, \kappa, \alpha) : \mathcal{S}_\alpha \to \mathcal{S}_\alpha$ by

$$P\left(x, b, \kappa, \alpha\right) := \varphi\left(T(\Delta(x), b, \kappa, \alpha), \Delta(x), b, \kappa\right). \tag{19}$$

Next let us define the standard basis for $\mathbb{R}^m$ as $\{e_i\}_{i=1}^m$. According to the construction procedure, for every $b = e_i$ and $\kappa = 0$, the nonholonomic output $y(q, \sigma_u, b, \kappa)$ is reduced to the holonomic output corresponding to the slope α_i, that is, $y(q, \sigma_u, e_i, 0) = h_{\text{h},\alpha_i}(q)$. Hence, we preserve the holonomic fixed point as follows:

$$P\left(x^\star_{\text{h},\alpha_i}, e_i, 0, \alpha_i\right) = x^\star_{\text{h},\alpha_i}, \quad \forall \alpha_i \in \mathcal{A}. \tag{20}$$

Now we are in a position to present the following theorem for the existence and stability of fixed points for the nonholonomic virtual constraints.

Theorem 1 (Existence and Stability of Periodic Orbits): There exists an open neighborhood of $(e_i, 0, \alpha_i)$, denoted by $\mathcal{N}(e_i, 0, \alpha_i)$, such that for all $(b, \kappa, \alpha) \in \mathcal{N}(e_i, 0, \alpha_i)$ the following statements hold:

1) There is a nonholonomic fixed point $x^\star_{\text{nh},b,\kappa,\alpha}$ for the Poincaré map, that is,
$$P\left(x^\star_{\text{nh},b,\kappa,\alpha}, b, \kappa, \alpha\right) = x^\star_{\text{nh},b,\kappa,\alpha}. \tag{21}$$
2) The fixed point $x^\star_{\text{nh},b,\kappa,\alpha}$ and the corresponding periodic orbit $\mathcal{O}_{\text{nh},b,\kappa,\alpha}$ are exponentially stable for the closed-loop hybrid system.

Proof: We apply the Implicit Function Theorem to the algebraic equation

$$F\left(x, b, \alpha, \kappa\right) := P\left(x, b, \kappa, \alpha\right) - x. \tag{22}$$

Since i) $F(x^\star_{\text{h},\alpha_i}, e_i, 0, \alpha_i) = 0$ and ii) from exponential stability of holonomic fixed points

$$\frac{\partial F}{\partial x}(x^\star_{\text{h},\alpha_i}, e_i, 0, \alpha_i) = \frac{\partial P}{\partial x}(x^\star_{\text{h},\alpha_i}, e_i, 0, \alpha_i) - I \tag{23}$$

is a nonsingular matrix, one can conclude the existence of $\mathcal{N}(e_i, 0, \alpha_i)$ on which Part 1 is satisfied. Part 2 is correct since i) the holonomic fixed points are exponentially stable, and ii) the elements of the Jacobian matrix $\frac{\partial P}{\partial x}(x, b, \kappa, \alpha)$ and thereby the eigenvalues are continuous with respect to (b, κ, α).

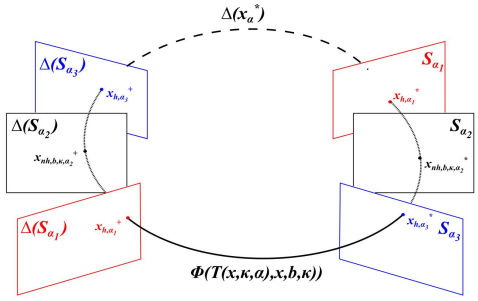

Fig. 2: Geometric interpretation of the optimization problem. Here (*) and (+) correspond to fixed point and post-impact, respectively.

From Theorem 1, we next formulate the following nonlinear optimization problem to find a unifying nonholonomic output.

Optimization Problem (NHVC-OP): Find b and κ such that the following conditions are met:

1) The flow extension map (i.e., solution) for the ordinary differential equation $\dot{x} = f^{\text{cl}}(x, b, \kappa)$ passes through all holonomic fixed points and their post impact states, i.e., for all $\alpha_i, \alpha_j \in \mathcal{A}$ with the property $\alpha_j < \alpha_i$,
$$\mathcal{F}\left(x^\star_{\text{h},\alpha_i}, b, \kappa, \alpha^\star_j\right) = x^\star_{\text{h},\alpha_j} \tag{24}$$
and for all $\alpha_i, \alpha_j \in \mathcal{A}$ with the property $\alpha_j > \alpha_i$,
$$\mathcal{F}\left(\Delta(x^\star_{\text{h},\alpha_i}), b, \kappa, \alpha^\star_j\right) = \Delta(x^\star_{\text{h},\alpha_j}). \tag{25}$$
2) The set of coefficients, b, are designed such that,
$$b_i \geq 0 \quad \text{and} \quad \sum b_i = 1. \tag{26}$$
3) The energy consumption $\int_0^T \|u(x, b, \kappa)\|^2 \mathrm{d}t$ is minimized over the entire solution.
4) The minimum normal ground reaction force is greater than 0 over the entire solution.
5) The maximum ratio of tangential to normal ground reaction forces is less than the static friction limit, $|F^T/F^N| < \mu_s$.

In the aforementioned optimization, the output parameters κ^* and b^* will define a nonholonomic output that prescribes the motion of the biped. The forces mentioned in constraints 4 and 5, are calculated throughout the continuous dynamics [23]. Essentially, we are minimizing the energy required over one step, while also enforcing that the nonholonomic output will pass through the fixed point of each Poincaré section (i.e. for all α_i). The result of this optimization are the coefficients κ^* and b^* that yield a nonholonomic walking gait for all terrain inclines.

Proposition 1 (Fixed Points for the Optimal System): Under conditions (24) and (25), the closed-loop hybrid system with the optimal coefficients κ^* and b^* has a periodic solution for every $\alpha_i \in \mathcal{A}$.

Proof: For every $\alpha_i \in \mathcal{A}$, let us take the fixed point $x^\star_{\text{h},\alpha_i} \in \mathcal{S}_{\alpha_i}$. Since the impact map Δ does not depend on α [28], the state solution of the closed-loop continuous-time dynamics $\dot{x} = f^{\text{cl}}(x, b^*, \kappa^*)$ will start from $\Delta(x^\star_{\text{h},\alpha_i})$

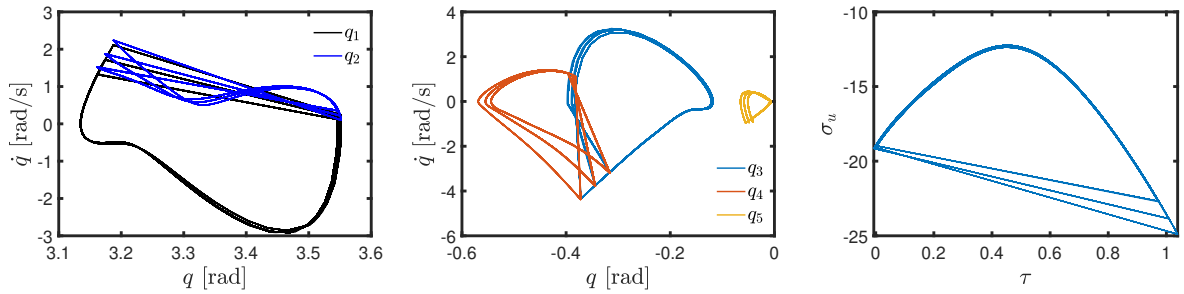

Fig. 3: The simulation results for the biped when subject to the predefined reference slope angles with transitions for the NHVC-OP control scheme: (a,b) the periodic orbits of the biped, and (c) the zero dynamics of the biped.

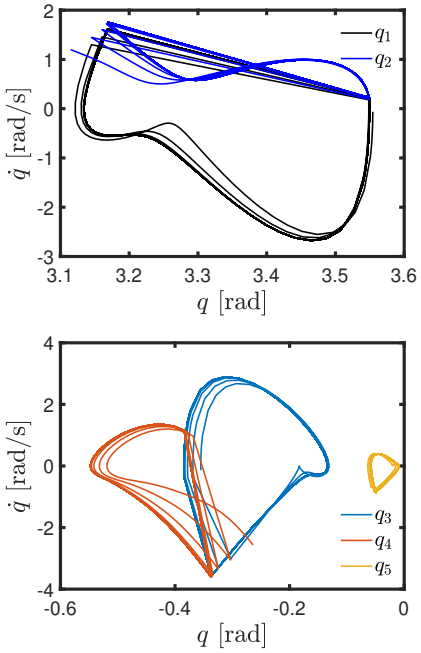

Fig. 4: The periodic orbits of the biped when subject to NHVC-OP control scheme, and a 5% uncertainty is present in the mass parameters of the biped.

and will pass through all fixed points (see (24) and (25)) until it hits the guard $\mathcal{S}_{\alpha_i}$ at $x^{\star}_{\mathrm{h},\alpha_i}$. Hence, $x^{\star}_{\mathrm{h},\alpha_i}$ is indeed a nonholonomic fixed point for the closed-loop hybrid system that corresponds to a periodic solution.

Remark: Under Proposition 1, the NHVC h_{nh} in (16), which is obtained by solving the optimization problem NHVC-OP, guarantees that stabilizing the output $y(q, \sigma_u, b, \kappa)$ given by (15) results in stable walking across a variety of terrains with different slopes *without any need for switching* among the stable VHC-based gaits $h_{\mathrm{h}_{\alpha_i}}$.

IV. Simulation Results

Having presented the method of NHVC design for multiple possible Poincaré sections, we now consider an example design for the five-link biped RABBIT. For the design phase, we define the finite set of reference slope angles as $\mathcal{A} = \{-2^{\circ}, 0^{\circ}, 2^{\circ}\}$. The nonholonomic output, parameterized by κ and b, is then designed to preserve the fixed points of the hybrid-invariant holonomic outputs for the uphill, level ground, and downhill cases. The `fmincon` function in MATLAB is used to compute the coefficients κ and the vector b. The time to solve this problem is approximately 20-30 minutes, using an Intel Core i7-4770 processor, due to the complexity of the dynamics and constraints. The solving time also depends on the design parameters (choice of holonomic gaits and slope disturbances), initial starting point of the optimization, and the tolerance selected for convergence. This model-based optimization technique is used for offline design of outputs, and we will demonstrate robustness of the resulting walking gait to model uncertainty in order to justify future experimental implementations. For this example, the output of the optimization will be noted as NHVC-OP. The biped RABBIT weighs $32kg$ and stands $1.425m$ tall. Detailed physical parameters of the biped RABBIT can be found in [23], [24] and have been omitted for brevity.

Given this NHVC design, we now simulate the biped for three separate cases. First, we simulate the biped walking exactly on the finite set of reference slope angles with transitions. Second, we will evaluate the performance of the proposed control strategy in the presence of parametric model uncertainties. Lastly, we submit the biped to randomly varying terrain corresponding to slopes outside the reference slope angles using both the ideal, rigid impact model and a compliant impact model to demonstrate robustness to nonparametric model uncertainties. A supplemental media file showing these simulations is available for download.

A. Optimization Designed NHVC

We first will present the results for the output of the optimization problem described in Sec. III. To do so, we simulate the biped for each of the three reference slope angles for ten meters. The terrain is designed such that the biped initializes on a slope parameterized by $\alpha_1 \in \mathcal{A}$. After ten meters, the terrain slope changes and is then parameterized by the next reference angle, $\alpha_2 \in \mathcal{A}$, for ten meters. The same transition occurs for the last reference angle for another ten meters. In Fig. 3 (a,b), the dynamic response of the biped for each joint angle is presented. Given the three slope conditions, the biped converges to three distinct periodic orbits with no transient behavior during transition

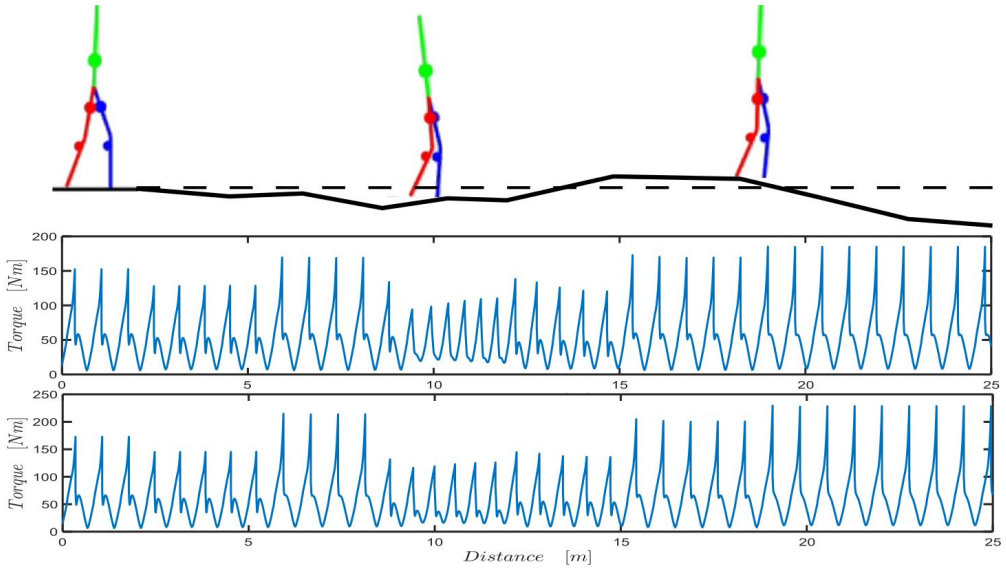

Fig. 5: The simulation results for the biped when subject to randomly varying terrain: (Top) an example terrain profile, (middle) the 2-norm of the torque applied to the biped when rigid ground impacts are present, and (bottom) the 2-norm of the torque applied to the biped when compliant ground impacts are present.

between orbits. This property is best highlighted by Fig. 3 (c) which illustrates the zero dynamics of the biped during the simulation. Note that each orbit passes through the impact point of the larger incline orbits, thereby allowing seamless transitions from one orbit to the next.

B. Robustness to Parametric Model Uncertainty

The NHVCs presented in this work are derived using the inertial matrix of the robot (i.e., $\sigma_u = B^{\perp} M(q)\dot{q}$) and assuming it is known exactly. In this subsection, we explore the sensitivity of our proposed approach when uncertainty exists in the model parameters. We will consider the scenario (commonly seen in practice) where inertial mass parameters used in simulation do not match the parameters used in the controller. To do this, we use the original parameters (mass values) for the NHVC control design and then change the physical parameters in the simulation.

In this simulation a 5% uncertainty in the mass values is applied to the biped. The biped is then simulated across level ground for a distance of 25 meters. Fig. 4 shows the performance of the biped and the eventual periodic orbit that is achieved. Comparing Fig. 4 with Fig. 3 (a,b), we note that in the presence of uncertainty the biped does not converge back to the same periodic orbit. However, the control scheme is robust enough to find a stable walking motion that accommodates the unknown physical parameters.

C. Robustness to Terrain Disturbances

In this section we will present simulation results for exposing the biped RABBIT [24] to randomly varying terrain changes with two simulated contact models. First, we will consider the rigid impact model with which the walking gait was optimized. Noting that walking surfaces are not perfectly rigid in the real world, we will also model the compliant impacts observed in practice to test the robustness of the proposed control law.

We begin by introducing the model used to simulate compliant ground interactions. The LuGre friction model is used to calculate the coefficient of friction [29], and the interface between the leg end and the ground is treated as contact between two bristles [1]. The dynamics are described by the full seven DOF model over the entire stride, even at impact which now has a nonzero duration. With this model, contact forces at the leg end are continuous, which means they will not experience an instantaneous jump to zero at transition [23], [30]. This compliant contact model represents nonparametric uncertainty in the idealized model-based design of the outputs in Sec. III.

We now detail the random terrain disturbance that is applied to the biped. Specifically, we subject the biped to a randomly varying terrain slope equipped with a compliant surface and compare the performance of the NHVC obtained from the optimization problem (NHVC-OP) with a VHC designed for level ground and the NHVC presented in [21] (NHVC-H). The simulation is designed such that the biped will walk for a maximum of 25 meters, and every 2 meters the slope of the terrain is changed randomly based on a uniform distribution. The terrain surface is generated offline and then simulated on the biped. Each terrain slope is a randomly selected real number between values of $-8^{\circ} \leq \alpha \leq 8^{\circ}$, which is four times the design range of NHVC-OP.

Each control scheme was simulated for the same set of 100 randomly generated terrain surfaces and contact models, and an example of a generated terrain surface is shown in Fig. 5. Fig. 5 (middle) details the 2-norm of the torque applied in the presence of rigid impacts, and Fig. 5 (bottom) shows the case of compliant impacts. For this experiment, the maximum observed peak torque of the system is 115 Nm. This peak torque is with in 15% of that reported by [1] (which uses the same RABBIT biped), and is an achievable torque level for a physical system [31].

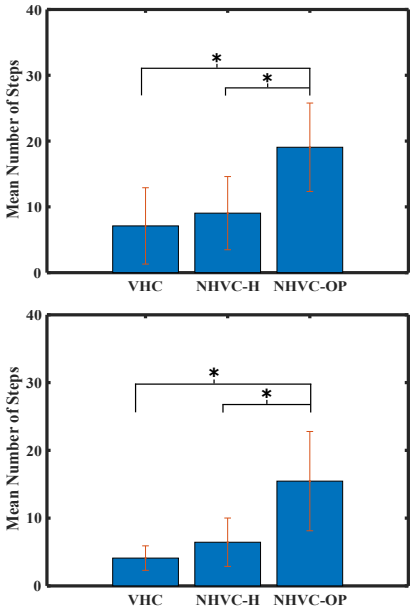

Fig. 6: Mean number of steps achieved over randomly varying terrain with rigid ground impacts (top), and with compliant impacts (bottom). Note * indicates $p < 0.05$.

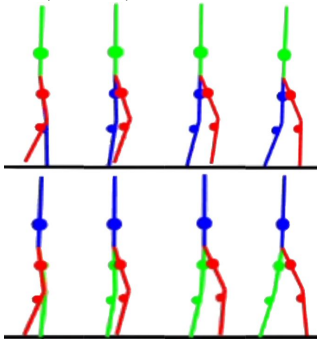

Fig. 7: Gait tiles for the biped subjected to the NHVC-OP control scheme (top), and the gait tiles for the biped subject to the NHVC-H control scheme (bottom).

After simulating the biped with each control scheme, the mean number of steps until failure or completion of 25 meters for rigid impacts was found as $\mu_{\text{VHC}} = 7.11 \pm 5.8$, $\mu_{\text{NHVC-H}} = 9.05 \pm 5.56$, and $\mu_{\text{NHVC-OP}} = 19.06 \pm 6.72$, and for compliant impacts was found as $\mu_{\text{VHC}} = 4.12 \pm 1.8$, $\mu_{\text{NHVC-H}} = 6.45 \pm 3.56$, and $\mu_{\text{NHVC-OP}} = 15.46 \pm 7.34$. Since each of the individual samples were not normally distributed, a Mann-Whitney U test was performed on the data set and showed that neither the VHC nor NHVC-H control schemes belong to the same population as the NHVC-OP controller. Fig. 6 illustrates the average number of steps for each control scheme and indicate significance when applicable for both simulators. This result shows that we can claim with 95% confidence that there exists a statistically significant difference between the NHVC-OP and both of the alternative control schemes, in both simulation environments.

D. Discussion

The improved robustness of the NHVC-OP control scheme is best illustrated through the gait tiles in Fig. 7, which shows the biped over level ground with NHVC-OP (top) and NHVC-H (bottom). We note that through the progression of one stride the NHVC-OP controller maintains greater foot clearance and a smaller stride length over the NHVC-H controller. This distinct difference in the NHVC-OP walking gait, which resembles a "marching" style gait, helps avoid foot scuffing and results in the NHVC-OP gait surviving randomly varying terrains better than the original NHVC gait (note foot scuffing is a route to failure during simulations). This characteristic arises as an indirect feature of the optimization problem formulation and is not directly designed behavior. However, this improved robustness does come with an associated cost. We consider the cost function [21],

$$\text{Cost} = \frac{1}{\text{step length}} \int_0^T ||u(t)||_2^2 dt. \tag{27}$$

For one step over level ground, we note that $\text{Cost}_{\text{NHVC-OP}} = 18.24\text{E}3$ and $\text{Cost}_{\text{NHVC-H}} = 6.29\text{E}3$. Therefore, the NHVC-OP control scheme inherently possesses a larger cost in order to achieve a more robust "marching" style walking gait. Designing NHVC-OP with a smaller slope range (e.g., $\pm 1°$) would provide a compromise between terrain robustness and cost of transport, somewhere in between the two studied cases.

Additionally, it is important to note that the type of varying terrain will affect the performance of the biped. For example, if the biped is exposed to a slope change progression that is always decreasing at regular increments, the NHVC-OP gait is able to reach slopes as high as $-15°$. However, the performance of the biped is directly linked to the inputs to the optimization problem. Incorporating additional constraints in the optimization problem can produce outputs specific to the user's desired performance.

From an implementation perspective, our method could be used on more complex humanoid robots (such as COMAN [32]) using a compact representation of the model equations. Furthermore, we believe the methods proposed in this work will indeed be applicable to physical humanoid robots based on the experimental results of Griffin [33]. In [33], Griffin showed that NHVCs can produce stable walking on the robot MARLO. Regarding the possibility of implementing our proposed NHVC-based walking gaits on existing assistive exoskeletons, e.g., [34], we believe that momentum-based gaits are well-suited for rehabilitation applications as they do not enforce restrictive kinematic constraints during the patient movements.

V. Conclusion and Future Research

In this paper, we extended a family of stable walking gaits, known as NHVCs, to realize stable variable-incline bipedal walking under a single, fixed controller. The design method considers a finite set of terrain slope disturbances, with a corresponding stable holonomic output for each slope, and seeks to preserve the fixed points of holonomic outputs through solving an off-line optimization problem. The synthesized controllers using the proposed NHVC method do not require explicit knowledge of the terrain to update the controller

parameters at each step; instead a single output encodes variable-incline locomotion. Using the proposed method, an NHVC was designed for the biped robot RABBIT by solving an optimization problem. The designed NHVCs were then simulated over terrain corresponding to the reference slope angles, a set of *random* terrain disturbances outside the set of reference slope angles, and for the practical scenario where uncertainties in the model information are present. The simulation results indicated a statistically significant improvement over the traditional VHC control scheme and the NHVC-H control scheme presented in [21].

For future research, we plan to investigate further the capability of designing NHVCs for other types of external disturbances. For example, it may be possible to design a unified NHVC for a continuum of inclines as opposed to a discrete set. Another future research direction will be to extend the current work to the design of nonlinear feedback controllers for powered prostheses, in order to restore normative human walking across various terrain profiles.

REFERENCES

[1] F. Plestan, J. W. Grizzle, E. R. Westervelt, and G. Abba, "Stable walking of a 7-dof biped robot," *IEEE Transactions on Robotics and Automation*, vol. 19, no. 4, pp. 653–668, 2003.

[2] B. Griffin and J. Grizzle, "Walking gait optimization for accommodation of unknown terrain height variations," in *2015 American control conference (ACC)*. IEEE, 2015, pp. 4810–4817.

[3] A. Hereid, C. M. Hubicki, E. A. Cousineau, and A. D. Ames, "Dynamic humanoid locomotion: A scalable formulation for hzd gait optimization," *IEEE Transactions on Robotics*, vol. 34, no. 2, pp. 370–387, 2018.

[4] K. Akbari Hamed, B. G. Buss, and J. W. Grizzle, "Exponentially stabilizing continuous-time controllers for periodic orbits of hybrid systems: Application to bipedal locomotion with ground height variations," *The International Journal of Robotics Research*, vol. 35, no. 8, pp. 977–999, 2016.

[5] C. O. Saglam and K. Byl, "Meshing hybrid zero dynamics for rough terrain walking," in *2015 IEEE International Conference on Robotics and Automation (ICRA)*. IEEE, 2015, pp. 5718–5725.

[6] R. D. Gregg, T. Lenzi, L. J. Hargrove, and J. W. Sensinger, "Virtual constraint control of a powered prosthetic leg: From simulation to experiments with transfemoral amputees," *IEEE Transactions on Robotics*, vol. 30, no. 6, pp. 1455–1471, 2014.

[7] H. Zhao, J. Reher, J. Horn, V. Paredes, and A. D. Ames, "Realization of stair ascent and motion transitions on prostheses utilizing optimization-based control and intent recognition," in *Rehabilitation Robotics (ICORR), 2015 IEEE International Conference on*. IEEE, 2015, pp. 265–270.

[8] D. Quintero, D. J. Villarreal, D. J. Lambert, S. Kapp, and R. D. Gregg, "Continuous-phase control of a powered knee–ankle prosthesis: Amputee experiments across speeds and inclines," *IEEE Transactions on Robotics*, vol. 34, no. 3, pp. 686–701, 2018.

[9] C. Liu, C. G. Atkeson, and J. Su, "Biped walking control using a trajectory library," *Robotica*, vol. 31, no. 2, pp. 311–322, 2013.

[10] R. Hartley, X. Da, and J. W. Grizzle, "Stabilization of 3D underactuated biped robots: Using posture adjustment and gait libraries to reject velocity disturbances," in *2017 IEEE Conference on Control Technology and Applications*, 2017, pp. 1262–1269.

[11] X. Da and J. Grizzle, "Combining trajectory optimization, supervised machine learning, and model structure for mitigating the curse of dimensionality in the control of bipedal robots," *The International Journal of Robotics Research*, vol. 38, no. 9, pp. 1063–1097, 2019.

[12] Q. Nguyen and K. Sreenath, "Exponential control barrier functions for enforcing high relative-degree safety-critical constraints," in *American Control Conference (ACC), 2016*. IEEE, 2016, pp. 322–328.

[13] Q. Nguyen, A. Agrawal, X. Da, W. C. Martin, H. Geyer, J. W. Grizzle, and K. Sreenath, "Dynamic walking on randomly-varying discrete terrain with one-step preview," in *Robotics: Science and Systems*, 2017.

[14] K. R. Embry, D. J. Villarreal, R. L. Macaluso, and R. D. Gregg, "Modeling the kinematics of human locomotion over continuously varying speeds and inclines," *IEEE Transactions on Neural Systems and Rehabilitation Engineering*, vol. 26, no. 12, pp. 2342–2350, 2018.

[15] H.-W. Park, A. Ramezani, and J. Grizzle, "A finite-state machine for accommodating unexpected large ground-height variations in bipedal robot walking," *IEEE Transactions on Robotics*, vol. 29, no. 2, pp. 331–345, 2013.

[16] B. Griffin and J. Grizzle, "Nonholonomic virtual constraints for dynamic walking," in *Decision and Control (CDC), 2015 IEEE 54th Annual Conference on*. IEEE, 2015, pp. 4053–4060.

[17] ——, "Nonholonomic virtual constraints and gait optimization for robust walking control," *The International Journal of Robotics Research*, vol. 36, no. 8, pp. 895–922, 2017.

[18] A. Hereid, S. Kolathaya, and A. D. Ames, "Online optimal gait generation for bipedal walking robots using Legendre pseudospectral optimization," in *Decision and Control (CDC), 2016 IEEE 55th Conference on*. IEEE, 2016, pp. 6173–6179.

[19] H. Diedam, D. Dimitrov, P.-B. Wieber, K. Mombaur, and M. Diehl, "Online walking gait generation with adaptive foot positioning through linear model predictive control," in *2008 IEEE/RSJ International Conference on Intelligent Robots and Systems*. IEEE, 2008, pp. 1121–1126.

[20] A. Herdt, H. Diedam, P.-B. Wieber, D. Dimitrov, K. Mombaur, and M. Diehl, "Online walking motion generation with automatic footstep placement," *Advanced Robotics*, vol. 24, no. 5-6, pp. 719–737, 2010.

[21] J. C. Horn, A. Mohammadi, K. Akbari Hamed, and R. D. Gregg, "Hybrid zero dynamics of bipedal robots under nonholonomic virtual constraints," *IEEE Control Systems Letters*, vol. 3, no. 2, pp. 386–391, 2019.

[22] K. Akbari Hamed and A. D. Ames, "Nonholonomic hybrid zero dynamics for the stabilization of periodic orbits: Application to underactuated robotic walking," *IEEE Transactions on Control Systems Technology*, pp. 1–8, 2019.

[23] E. R. Westervelt, J. W. Grizzle, C. Chevallereau, J. H. Choi, and B. Morris, *Feedback Control of Dynamic Bipedal Robot Locomotion*. Boca Raton: CRC Press, Jun. 2007.

[24] C. Chevallereau, G. Abba, Y. Aoustin, F. Plestan, E. Westervelt, C. C. de Wit, and J. Grizzle, "Rabbit: A testbed for advanced control theory," *IEEE Control Systems Magazine*, vol. 23, no. 5, pp. 57–79, 2003.

[25] R. M. Murray, Z. Li, and S. S. Sastry, *A Mathematical Introduction to Robotic Manipulation*. Boca Raton: CRC Press, Mar. 1994.

[26] Y. Hürmüzlü and D. B. Marghitu, "Rigid body collions of planar kinematic chains with multiple contact points," *Intl. J. of Robotics Research*, vol. 13, no. 1, pp. 82–92, Feb. 1994.

[27] E. R. Westervelt, J. W. Grizzle, and D. E. Koditschek, "Hybrid zero dynamics of planar biped walkers," *IEEE TAC*, vol. 48, no. 1, pp. 42–56, Jan. 2003.

[28] M. W. Spong and F. Bullo, "Controlled symmetries and passive walking," *IEEE TAC*, vol. 50, no. 7, pp. 1025–1031, 2005.

[29] C. C. De Wit, H. Olsson, K. J. Astrom, and P. Lischinsky, "A new model for control of systems with friction," *IEEE Transactions on automatic control*, vol. 40, no. 3, pp. 419–425, 1995.

[30] K. A. Hamed and R. D. Gregg IV, "Decentralized event-based controllers for robust stabilization of hybrid periodic orbits: Application to underactuated 3-d bipedal walking," *IEEE Transactions on Automatic Control*, vol. 64, no. 6, pp. 2266–2281, 2018.

[31] T. Elery, S. Rezazadeh, C. Nesler, J. Doan, H. Zhu, and R. D. Gregg, "Design and benchtop validation of a powered knee-ankle prosthesis with high-torque, low-impedance actuators," in *2018 IEEE International Conference on Robotics and Automation (ICRA)*. IEEE, 2018, pp. 2788–2795.

[32] L. Colasanto, N. G. Tsagarakis, and D. G. Caldwell, "A compact model for the compliant humanoid robot coman," in *2012 4th IEEE RAS & EMBS International Conference on Biomedical Robotics and Biomechatronics (BioRob)*. IEEE, 2012, pp. 688–694.

[33] J. W. Grizzle and C. Chevallereau, "Virtual constraints and hybrid zero dynamics for realizing underactuated bipedal locomotion," *arXiv preprint arXiv:1706.01127*, 2017.

[34] L. Saccares, A. Brygo, I. Sarakoglou, and N. G. Tsagarakis, "A novel human effort estimation method for knee assistive exoskeletons," in *2017 International Conference on Rehabilitation Robotics (ICORR)*. IEEE, 2017, pp. 1266–1272.